Biological Cybernetics (2024) 118:21–37
https://doi.org/10.1007/s00422-024-00984-1

Biological Cybernetics

ORIGINAL ARTICLE

EEG rhythm separation and time–frequency analysis of fast multivariate empirical mode decomposition for motor imagery BCI

Yang Jiao[1,4] · Qian Zheng[1] · Dan Qiao[2] · Xun Lang[3] · Lei Xie[2] · Yi Pan[1]

Received: 22 May 2023 / Accepted: 11 February 2024 / Published online: 12 March 2024

Abstract

Motor imagery electroencephalogram (EEG) is widely employed in brain–computer interface (BCI) systems. As a time–frequency analysis method for nonlinear and non-stationary signals, multivariate empirical mode decomposition (MEMD) and its noise-assisted version (NA-MEMD) has been widely used in the preprocessing step of BCI systems for separating EEG rhythms corresponding to specific brain activities. However, when applied to multichannel EEG signals, MEMD or NA-MEMD often demonstrate low robustness to noise and high computational complexity. To address these issues, we have explored the advantages of our recently proposed fast multivariate empirical mode decomposition (FMEMD) and its noise-assisted version (NA-FMEMD) for analyzing motor imagery data. We emphasize that FMEMD enables a more accurate estimation of EEG frequency information and exhibits a more noise-robust decomposition performance with improved computational efficiency. Comparative analysis with MEMD on simulation data and real-world EEG validates the above assertions. The joint average frequency measure is employed to automatically select intrinsic mode functions that correspond to specific frequency bands. Thus, FMEMD-based classification architecture is proposed. Using FMEMD as a preprocessing algorithm instead of MEMD can improve the classification accuracy by 2.3% on the BCI Competition IV dataset. On the Physiobank Motor/Mental Imagery dataset and BCI Competition IV Dataset 2a, FMEMD-based architecture also attained a comparable performance to complex algorithms. The results indicate that FMEMD proficiently extracts feature information from small benchmark datasets while mitigating dimensionality constraints resulting from computational complexity. Hence, FMEMD or NA-FMEMD can be a powerful time–frequency preprocessing method for BCI.

Keywords Fast multivariate empirical mode decomposition (FMEMD) · Time–frequency analysis · Electroencephalogram · Rhythm Separation · Motor imagery

1 Introduction

Motor imagery, based on brain–computer interface (BCI) systems that establish direct communication between the human brain and communication devices, provides users with the ability to control computer cursors, interactive robotic wheelchairs, and explore virtual environments (Doud et al. 12). Among various brain imaging measurements used in BCI, electroencephalogram (EEG) is widely used for the classification of motor imagery tasks due to its low cost and noninvasive nature (Lebedev and Nicolelis 26). However, inferring the category of actions that the subject is imagining based on raw EEG signals is not easy, as they contain cross-channel interdependence of multichannel data, strong nonstationary characteristics, low signal-to-noise ratio (SNR), and other hard-to-analyze features (Graimann 14, Park et al. 38, Wang et al. 55). Therefore, a general approach

Communicated by Benjamin Lindner.

✉ Qian Zheng
q.zheng@siat.ac.cn

✉ Yi Pan
yi.pan@siat.ac.cn

1 Shenzhen Institute of Advanced Technology, Chinese Academy of Sciences, Shenzhen 518026, China

2 State Key Laboratory of Industrial Control Technology, Zhejiang University, Hangzhou 310027, China

3 Department of Electronic Engineering, Information School, Yunnan University, Kunming 650091, China

4 University of Nottingham Ningbo China, Ningbo 315100, China

for motor imagery classification with EEG data involves four steps: (1) pre-processing; (2) feature extraction; (3) feature selection; (4) learning a classifier. Although deep learning methods that are recently used for the classification of motor imagery tasks (Dai et al. 9, Tabar and Halici 51, Zhang et al. 58) can achieve the above procedures simultaneously, they still require preprocessing approaches to enhance the related features of EEG signals (Craik et al. 8, Hernández and Antelis 15, Wang et al. 55).

Over the past two decades, several techniques have been proposed for the preprocessing and feature extraction of motor imagery signals. These methods are based on the neurophysiological changes of EEG signals in specific frequency bands, such as the *mu* (8–12 Hz) and *beta* (18–25 Hz) rhythms, when subjects plan and execute hand or finger movements. Specifically, during motor imagery, the *mu* or *beta* rhythm exhibits the event-related decrease (ERD) over the contralateral scalp and the event-related increase (ERS) over the ipsilateral area, as observed in previous studies (Yuan and He 56). These changes in the *mu* and *beta* rhythms are then extracted and quantified by the preprocessing and feature extraction methods.

In the preprocessing stage, most methods are based on existing signal processing technologies (Graimann 14, Kevric and Subasi 20, Nicolas-Alonso and Gomez-Gil 36, Pfurtscheller et al. 41). For example, [41, 42] utilize the Fourier transform to analyze and filter EEG data for each channel. However, due to the nonlinear and non-stationary of EEG data, several researchers have explored the use of the wavelet transform to separate the original data into diverse frequency sub-bands, thereby enhancing the features of specific rhythms (Mousavi et al. 35, Robinson et al. 47). Despite their usefulness, classical signal processing methods, including Fourier and wavelet transforms, are limited by a predefined set of basis functions and cannot provide highly centralized time–frequency representations of EEG data (Park et al. 38). Therefore, empirical mode decomposition (EMD), a fully data-driven time–frequency analysis technique, has also been explored by researchers for the preprocessing of EEG data (Wang et al. 54).

After the preprocessing stage, feature extraction methods are used to quantify the filtered signals. These methods include Common Spatial Patterns (CSP) (Ramoser et al. 43), energy entropy (Hu et al. 16), adaptive autoregressive models (Anderson et al. 2), and wavelet transform coefficients (Bostanov and Kotchoubey 7). Note that several previously published studies combine preprocessing and feature extraction methods into an integrated framework, which are also referred to as hybrid technologies for feature extraction. For instance, Common Spatio-Spectral Pattern (CSSP) optimizes a simple filter that employs a one-time delayed sample with CSP algorithm (Lemm et al. 27). Additionally, Ang et al. propose the Filter Bank Common Spatial Pattern (FBCSP), which combines the bandpass filter bank with the CSP method to achieve feature extraction (Ang et al. 3).

However, the above-mentioned methods analyze or filter the signal from each EEG channel separately, without considering cross-channel interdependence, resulting in a problem of uniqueness: the decomposed components for each channel do not correspond in number and frequency (Mandic et al. 33, Park et al. 40). To address this issue, one widely used method is multivariate mode decomposition (MEMD) and its noise-assisted version (NA-MEMD) (Rehman and Mandic 44, Ur Rehman and Mandic 53). [38] have proposed a MEMD-based CSP approach for motor imagery classification, which fully benefits from its enhanced localization properties, the use of cross-channel information, and improved robustness to noise and artificial interferences. Inspired by this work, other studies have focused on improving classification accuracy and extending motor imagery tasks to multiple classes using similar MEMD-based frameworks (Bashar and Bhuiyan 4, Gaur et al. 13). However, the core algorithm, MEMD, still exposes several unsolved problems: (1) MEMD requires excessively high computational resources, especially for multivariate data (such as multichannel EEG) (Lang et al. 24, Rehman et al. 45); (2) The filter bank structure contained in MEMD is not stable enough and is vulnerable to measurement noise and interferences, leading to possible inaccurate decomposition behaviors like mode mixing (Lang et al. 24). Therefore, it is challenging for MEMD-based methods to be compatible with brain–computer interface (BCI) devices and practical rehabilitation medical environments.

To address these aforementioned problems, this paper explores the use of fast multivariate empirical mode decomposition (FMEMD) to analyze motor imagery responses. FMEMD is a computationally less-expensive alternative to MEMD that operates by applying univariate EMD on projected signals to obtain a set of intrinsic mode functions (IMFs). These IMFs are combined with their corresponding direction vectors and solved by a least square algorithm to yield Multivariate IMFs (MIMFs) (Lang et al. 24). FMEMD offers enhanced computational efficiency and a fairly stable filter bank property, making it highly robust to noise when processing low-SNR EEG data. Therefore, this paper proposes the FMEMD-based architecture for motor imagery tasks fully utilizing the benefits of FMEMD in terms of computational complexity and noise robustness.

Our proposed approach automatically eliminates redundant frequency bands and selects valuable ones by calculating the center frequencies of each decomposed component, thereby improving the characterization of brain activity. A comparative analysis between FMEMD and MEMD using simulation signals, similar to rhythms, confirms the superiority of FMEMD.

In addition, classification experiments conducted on two representative small datasets indicate that the FMEMD

scheme is proficient in augmenting data features on small multichannel datasets and can mitigate dimensionality constraints caused by computational complexity. It can also function as a general preprocessing filtering algorithm for adaptive EEG rhythm separation and can be integrated with other complex classification models including deep learning method to enhance the accuracy and robustness of the underlying models.

This paper is organized as follows: Sect. 2 introduces MEMD, FMEMD, and their noise-assisted versions. Section 3 illustrates the advantages of FMEMD compared to MEMD using two simulation cases. In Sect. 4, a brief introduction of a representative dataset is provided, and the time–frequency analysis of bi-channel EEG data using FMEMD and other existing methods are presented. Finally, Sect. 5 presents a complete FMEMD-based classification scheme, combining some basic feature extraction and classifiers. In Section 6, an overall conclusion is presented, summarizing the contributions and significance of the proposed FMEMD-based classification scheme for motor imagery tasks

2 Preliminaries

2.1 Multivariate empirical mode decomposition

Empirical mode decomposition (EMD) is a fully data-driven method used for analyzing nonlinear and non-stationary signals (Huang et al. 17). It decomposes a signal into a finite set of intrinsic mode functions (IMFs) that represent AM/FM components in nature. An IMF must satisfy two conditions: (1) the difference between the number of extrema and the number of zero crossings should be no more than one, and (2) the mean of the upper and lower envelopes defined by the local extrema should be close to zero. However, EMD is only applicable for univariate data.

To overcome this limitation, multivariate empirical mode decomposition (MEMD) was developed to analyze multivariate data (Mandic et al. 33, Rehman and Mandic 44, Rilling et al. 46). In MEMD, the estimation of the multivariate local mean is a critical step, as the concept of local extrema is not well-defined for multivariate signals. Following the similar idea in bivariate empirical mode decomposition (BEMD) (Rilling et al. 46), the MEMD algorithm uses real-valued projections along a set of directions on hyperspheres to obtain the extrema of multivariate signals. These extrema are then interpolated channel-wise to yield the desired envelopes. The multichannel local mean is finally estimated by averaging these envelopes. To improve the approximation accuracy of the local mean, MEMD utilizes quasi-Monte Carlo-based low-discrepancy sequences to generate a suitable set of direction vectors.

The MEMD method is summarized in Algorithm 1.

Algorithm 1 Multivariate empirical mode decomposition.

Input: $\mathbf{x}_1(t) = \mathbf{x}_2(t) = \mathbf{x}(t), i = 1;$

1: Generate a K uniformly distributed θ_k.
2: Calculate the kth projection $q^{\theta_k}(t)$ of the input $\mathbf{x}_1(t)$ as $q^{\theta_k}(t) = \mathbf{x}_1(t) \cdot (\mathbf{v}^{\theta_k})^T$, for all k ($k = 1, 2, \ldots, K$);
3: Find time instants $\left\{t_i^{\theta_k}\right\}$, which correspond to maxima of the projected signals $q^{\theta_k}(t)$ for all k;
4: Interpolate $\left[t_i^{\theta_k}, \mathbf{x}_1\left(t_i^{\theta_k}\right)\right]$ to obtain the multivariate envelope $\mathbf{e}^{\theta_k}(t)$;
5: For a set of K direction vectors, the mean of envelope curves, $\mathbf{m}(t)$, is given by

$$\mathbf{m}(t) = \frac{1}{K}\sum_{k=1}^{K}\mathbf{e}^{\theta_k}(t). \tag{1}$$

6: Extract the detail signal $\mathbf{s}(t)$ using $\mathbf{s}(t) = \mathbf{x}_1(t) - \mathbf{m}(t)$. If the detail signal satisfies the stopping criterion of MIMF, $\mathbf{d}_i(t) = \mathbf{s}(t)$, go to step 7. Otherwise $\mathbf{x}_1(t) = \mathbf{s}(t)$, go to step 2;
7: Update $\mathbf{x}_2(t) = \mathbf{x}_2(t) - \mathbf{d}_i(t)$. If $\mathbf{x}_2(t)$ becomes monotonic, or does not contain enough extrema to form a meaningful multivariate envelope, stop the above sifting process, and obtain the trend $\mathbf{r}(t) = \mathbf{x}_2(t)$. Otherwise, let $i = i + 1$ and $\mathbf{x}_1(t) = \mathbf{x}_2(t)$, go to step 2.
8: **return** $\{\mathbf{d}_i(t)\}_{i=1}^{M}$ and $\mathbf{r}(t)$.

The sifting process of a multivariate IMF can be stopped when all K projections of the detail signal $\mathbf{s}(t)$ satisfy the aforesaid stoppage criterion of the standard EMD. As a result, MEMD decomposes a p-variate signal $\mathbf{x}(t)$ as

$$\mathbf{x}(t) = \sum_{i=1}^{M}\mathbf{d}_i(t) + \mathbf{r}(t), \tag{2}$$

where the p-variate MIMFs, $\{\mathbf{d}_i(t)\}_{i=1}^{M}$, contain scale-aligned intrinsic joint rotational modes (Rehman and Mandic 44).

Researchers have demonstrated that MEMD enables cross-channel time–frequency analysis and provides high localization of specific frequency components (Gaur et al. 13, Mandic et al. 33, Park et al. 38). In a BCI study based on motor imagery EEG responses, the MEMD algorithm enhanced multicomponent extraction of the *mu* and *beta* rhythms of interest. In particular, the noise-assisted version of MEMD (NA-MEMD) allows for a more stable estimation of time–varying frequency information from multichannel EEG signals. Despite the powerful capability of MEMD for analyzing EEG data, there are several obstacles that limit its

usefulness for clinical applications, most notably its computational inefficiency when processing multichannel data.

Since MEMD performs cubic spline interpolations in each data channel for a single sifting process, its computational complexity increases as the total number of data channels increases (Lang et al. 24). Therefore, it is difficult to achieve real-time analysis and discrimination of motor imagery behaviors using multichannel EEG data. Additionally, the filter bank property of MEMD is not stable enough for noise disturbances. Therefore, even though using NA-MEMD, the mode mixing problem[1] (poor signal separation phenomenon) still arises in low-SNR complex signals like EEG. In the following section, we introduce the FMEMD algorithm and its noise-assisted version, which will be proven to overcome these problems and used to analyze the time–frequency variation of EEG data.

2.2 Fast multivariate empirical mode decomposition

FMEMD is a recently introduced method that has been shown to outperform MEMD in processing multivariate data with less computational cost. It operates by applying univariate EMD on projected signals to obtain a set of IMFs, which are combined with their corresponding direction vectors and then solved by a least squares algorithm to yield multivariate IMFs (MIMFs) (Lang et al. 24). The details of FMEMD are listed in Algorithm 2.

Algorithm 2 Fast multivariate empirical mode decomposition.

Input: $\mathbf{x}_1(t) = \mathbf{x}(t), i = 1$

1: Generate a suitable point set for uniform projection;
2: Calculate the kth projection $f^{\theta_k}(t)$ of the input signal $\mathbf{x}_1(t)$ along direction vector $\mathbf{v}^{\theta_k}$, for all k (i.e. $k = 1, 2, \ldots, K$, where K gives the whole set of vectors);
3: Extract the first univariate IMF $d^{\theta_k}(t)$ of the projected function $f^{\theta_k}(t)$ for all k using EMD algorithm (Huang et al. 17);
4: Combine all IMFs $\left\{d^{\theta_k}(t)\right\}_{k=1}^{K}$ with their corresponding direction vectors $\left\{\mathbf{v}^{\theta_k}\right\}_{k=1}^{K}$, the p-variate MIMF $\mathbf{d}_i(t)$ is obtained by solving the overdetermined equations

$$\left\{d^{\theta_k}(t)\right\}_{k=1}^{K} = \mathbf{d}_i(t) \cdot \left\{\mathbf{v}^{\theta_k}\right\}_{k=1}^{K}. \tag{3}$$

5: Calculate the slower mean $\mathbf{s}(t) = \mathbf{x}_1(t) - \mathbf{d}_i(t)$;
6: If $\mathbf{s}(t)$ does not contain enough extrema to form meaningful envelopes, stop the iterative process and obtain the trend, $\mathbf{r}(t) = \mathbf{s}(t)$. Otherwise, update the current input as $\mathbf{x}_1(t) = \mathbf{s}(t)$ and $i = i + 1$, then go to step 2;
7: **return** $\{\mathbf{d}_i(t)\}_{i=1}^{M}$ and $\mathbf{r}(t)$;

The stopping criterion used for univariate IMF extraction in step 3 is borrowed from (Huang et al. 18), where the sifting is stopped when the number of zero crossings and extrema is the same number for S successive sifting steps. Typically, a value of $S = 5$ has proved successful as the default stopping criterion.

Similar to the noise-assisted MEMD (NA-MEMD), we here add the extra noise channels into the original signal, and utilize FMEMD to decompose the synthesized signal, thereby eliminating the mode mixing. The noise-assisted FMEMD (NA-FMEMD) forces the alignment of multivariate IMFs (MIMFs) based on the dyadic filter structure of FMEMD, where each MIMF carries only one frequency sub-band. As mentioned before, compared with MEMD, FMEMD contains a much more stable filter bank property, thereby exhibiting stronger robustness to noise. Hence, it is more effective for NA-FMEMD to more effectively solve the mode mixing problem than NA-MEMD, which will be illustrated in the following experiments. The details of the noise-assisted version are outlined in Algorithm 3.

Algorithm 3 Noise-assisted Version of FMEMD.

Input: $\mathbf{x}(t) = \left[x_1(t), \ldots, x_p(t)\right]$

1: Create a q-channel uncorrelated white Gaussian noise $\mathbf{n}(t) = \left[n_1(t), \ldots, n_q(t)\right]$, with amplitude of σ;
2: Append the noise to the input, obtaining an $(p+q)$-variate composed signal, $\mathbf{c}(t) = [\mathbf{x}(t), \mathbf{n}(t)]$;
3: Obtain a set of MIMFs $\left\{\mathbf{d}_i^{\mathbf{c}}(t) = \left[\mathbf{d}_i^{\mathbf{x}}(t), \mathbf{d}_i^{\mathbf{n}}(t)\right]\right\}_{i=1}^{M}$ and a final trend $\mathbf{r}^{\mathbf{c}}(t) = \left[\mathbf{r}^{\mathbf{x}}(t), \mathbf{r}^{\mathbf{n}}(t)\right]$ through processing the signal $\mathbf{c}(t)$ by the FMEMD algorithm;
4: Discard the q-channel results corresponding to the noise, gaining MIMFs $\left\{\mathbf{d}_i^{\mathbf{x}}(t)\right\}_{i=1}^{M}$ and the trend $\mathbf{r}^{\mathbf{x}}(t)$.
5: **return** $\left\{\mathbf{d}_i^{\mathbf{x}}(t)\right\}_{i=1}^{M}$ and $\mathbf{r}^{\mathbf{x}}(t)$;

3 Comparative analysis on simulation signals

According to the previously published works (Park et al. 37,38, Rehman and Mandic 44), researchers have designed two representative simulation experiments on basis of multichannel low-SNR data like EEG for illustrating the ability of MEMD to extract the cross-channel information and the robustness to noise disturbance. These two experiments

[1] The mode mixing problem is defined as a signal IMF either consisting of signals of widely disparate scales, or a signal of a similar scale residing in different IMFs (Ur Rehman and Mandic 53). The NA-MEMD method can effectively alleviate the mode mixing since it enforces the signal decomposition process based on the quasi-dyadic filter bank structure of MEMD.

are called as the extraction of common oscillatory modes and component estimation, respectively. In fact, MEMD performs better in these experiments compared with the univariate method EMD (Park et al. 38). As mentioned before, FMEMD scheme exhibits a fairly stable filter bank structure and low computational complexity. In this section, we replicate the aforementioned experiments to illustrate that FMEMD framework exhibits a more precise, resilient, and efficient analysis on simulation oscillatory data, which is similar to EEG rhythms, as compared to MEMD. Moreover, it can serve as a general preprocessing filtering algorithm for adaptive EEG rhythm separation.

3.1 Common oscillatory modes of multivariate IMFs

We apply NA-MEMD and NA-FMEMD to a 3-channel synthetic signal to visually investigate the capability of FMEMD on the extraction of common oscillatory modes compared with that of MEMD. We choose the noise-assisted versions of MEMD and FMEMD since these two algorithms can effectively alleviate the mode mixing problem.

Note that the number of noise-assisted channels is set to 4. The Halton and Hammersley sequence is used for generating a set of $K = 64$ directions. The stoppage criterion is $S = 5$, and end effects are eliminated in advance. The simulation signal $[x_1(t), x_2(t), x_3(t)]$ is constructed by,

$$\begin{aligned} x_1(t) &= \begin{cases} 2\sin(2\pi f_1 t), t = 1, \ldots, 400 \\ 2\sin(2\pi f_1 t) + 1.5\sin(2\pi f_3 t), t = 401, \ldots, 1000 \end{cases} \\ x_2(t) &= 2\sin(2\pi f_1 t) + 2\sin(2\pi f_2 t), t = 1, \ldots, 1000 \\ x_3(t) &= \begin{cases} 2\cos(2\pi f_1 t), t = 1, \ldots, 600 \\ 2\sin(2\pi f_2 t), t = 601, \ldots, 1000 \end{cases} . \end{aligned} \tag{3}$$

where the sample frequency is $f_s = 1000$, and the frequencies of the signal are as follows: $f_1 = \frac{6}{f_s}$, $f_2 = \frac{15}{f_s}$, $f_3 = \frac{40}{f_s}$.

The time–domain decomposition results are shown in Figs. 1 and 2. As we can see that the common oscillatory modes are aligned at the same IMF level, where the $6Hz$ frequency mode, common to the three channels, is aligned by NA-MEMD at the d_9 in Fig. 1. However, NA-MEMD still generates the mode mixing problem, which is observed in d_7 and d_8 of Fig. 1. MIMFs extracted by NA-FMEMD in Fig. 2, by contrast, fully eliminate the mode mixing and are accurately located within different frequency scales. This illustrates that the performance of NA-FMEMD achieves a further improvement over NA-MEMD in terms of alleviating mode mixing problems, indicating that the FMEMD-based method enables a more accurate and unified frequency-band separation across the data channels, which is crucial for the analysis of multichannel EEG data.

We need to highlight that a robust filter bank property is the internal cause of stably reducing mode mixing phenomenons. More specifically, the intermittency and the randomness of

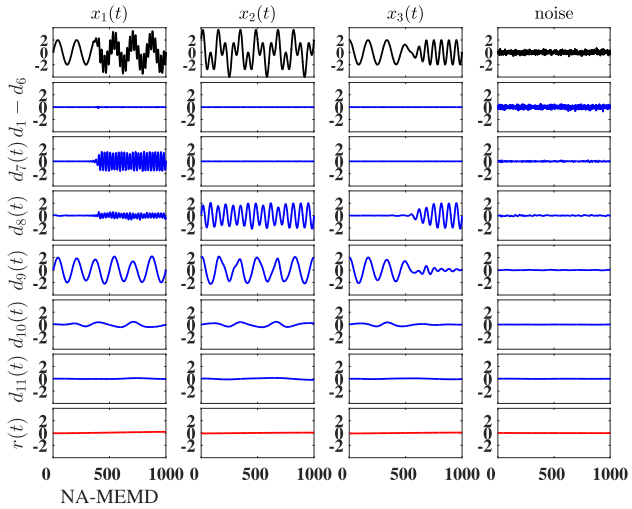

Fig. 1 The results decomposed by NA-MEMD. The mode mixing problem is present in d_7 and d_8

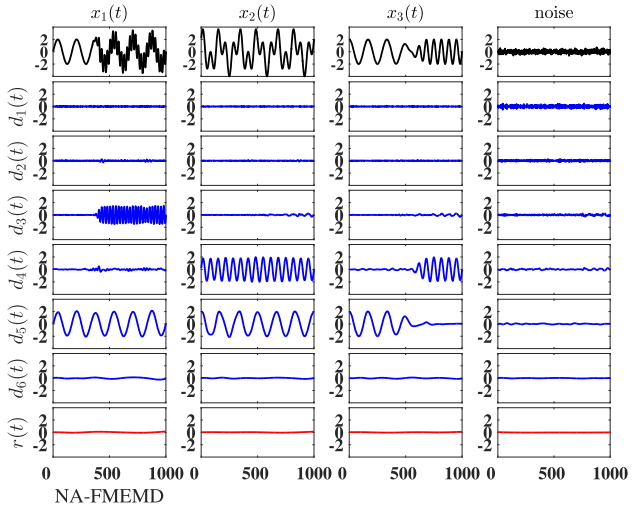

Fig. 2 The results decomposed by NA-FMEMD. Different frequency modes are separated to the corresponding MIMFs without mode mixing

multivariate multi-component signals easily lead to the aliasing among frequency sub-bands of the filter bank, which means that NA-MEMD cannot well recover high or low-frequency oscillations of the original signal. In comparison, FMEMD utilizes its fairly stable filter bank property to eliminate mode mixing with a noise-assisted framework. This enhanced capability of FMEMD that comes from the stability of the filter bank structure will be more prominently verified in the following experiment, component estimation.

3.2 Component estimation

In this section, we conduct the component estimation experiment to illustrate the improved noise robustness and higher computational efficiency of FMEMD compared with

MEMD. The simulation data is a multichannel signal where all channels contain the same one-component signal s_f, added by different realizations of white Gaussian noise (WGN), as shown below

$$x_1 = s_f + n_1, x_2 = s_f + n_2, \\ x_3 = s_f + n_3, \ldots, x_P = s_f + n_P. \quad (4)$$

where n_P represents a realization of WGN in the Pth channel. In this case, s_f represents one fixed sinusoidal signal (with the frequency 6 Hz or 15 Hz) common to all channels. We obtain a set of simulation signals by increasing the number of channels P from 4 to 8 and selecting diverse signal-to-noise ratios (SNRs) of 5 dB, 0 dB and -5 dB with respect to s_f. Each signal is decomposed by MEMD and FMEMD for 50 trials (corresponding to 50 noise realizations of each signal), and we select all specific MIMFs where contain the same frequency with s_f as the reconstructed sinusoidal signals. To conduct the performance assessment, we compute the mean and variance of new SNRs of these reconstructed signals, and provide the visual results by error bars. In addition, the sampling frequency is 1000 Hz and each trial lasts for 1 s. The parameters used in MEMD and FMEMD keep consistent with the previous experiment.

The estimation results are shown in Figs. 3 and 4, corresponding to the 6 Hz and 15 Hz frequency component, respectively. As can be seen that FMEMD outperforms MEMD for almost all input SNRs under different total numbers of channels.

Particularly, the estimation accuracies (the output SNRs) of MEMD significantly decrease when the input noises increase (SNRs from 5 to -5 dB), while FMEMD still maintains a consistent performance. In addition, for 50 repeated decomposition trials of each simulation signal, the output SNRs obtained by FMEMD show the fluctuations (variances) in a much smaller range than MEMD. This again verifies that FMEMD presents a fairly stable filter band structure, exhibiting the stronger robustness to different noise disturbances, resulting in a more accurate component estimation.

We also calculate the average running times of MEMD and FMEMD with respect to diverse numbers of data channels when extracting the common sinusoidal signals s_f by these two methods. The results are shown in Fig. 5. Observe that the computational efficiency of FMEMD to extract the cross-channel information is greatly improved compared with MEMD. This phenomenon will become much more striking if the total number of data channels increases, for instance, the computational time (59.3 s) of MEMD is nearly 30 times than that (2.5 s) of FMEMD when the 8-channel simulation data is decomposed for obtaining the 6 Hz sinusoidal signals.

4 Time–frequency analysis of EEG data

The section verifies the time–frequency analysis ability of FMEMD on practical EEG data. More specifically, we employ NA-FMEMD to detect ERD (event-related decrease) and ERS (event-related increase) phenomenons in the contralateral and the ipsilateral somatosensory cortex. The previously published work has illustrated that MEMD produces more accurate spectrogram estimations of EEG data over the classic univariate methods, such as the short-time Fourier transform (STFT) and continuous wavelet transform (CWT) (Park et al. 37,38,40). In this work, we conduct the comparison between NA-FMEMD and NA-MEMD in terms of the extraction of ERD and ERS, thereby illustrating that FMEMD is a more suitable method for the time–frequency analysis of EEG data.

4.1 Materials

We here make use of publically available BCI Competition IV Dataset I to select the EEG data to be analyzed (Blankertz et al. 5). The dataset was provided by the Berlin BCI group. EEG signals were recorded using 59 electrodes from four healthy subjects (a, b, f, and g). For each subject two classes of motor imagery were selected from three tasks. More precisely, subjects a and f performed left hand and foot motor imagery while subjects b and g carried out left hand and right hand motor imagery. A total of 200 trials were available for each subject, including 100 trials for each class.

In each trail, the visual cues are displayed in the computer screen for a period of 4 s during which the subject is instructed to perform one of the possible tasks. A 2 s blank screen and a 2 s fixed cross in the center of the screen are followed after the 4 s motor imagery task. The EEG signals are sampled at the sampling frequency of 100 Hz. For more details about BCI Competition IV Dataset I refer to (Blankertz et al. 5). According to the simulation results in Sect. 3.2, the computational efficiency of FMEMD almost gets rid of the influence of the data channel. Hence, we directly apply FMEMD to each EEG data with total 59 channels. For verifying how the number of processed channels affects the FMEMD performance using real-world EEG data, we have also considered 11 channels from the 59 EEG channels, "FC3", "FC4", "Cz", "C3", "C4", "C5", "C6", "T7", "T8", "CCP3", and "CCP4", and 4 channels from these 11 channels, "C3", "C4", "CCP3" and "CCP4", which are followed by [38]. Next, the ERD and ERS phenomenons on the left hand motor imagery datasets of subject g from electrode "C3" and "C4" are estimated using FMEMD and MEMD.

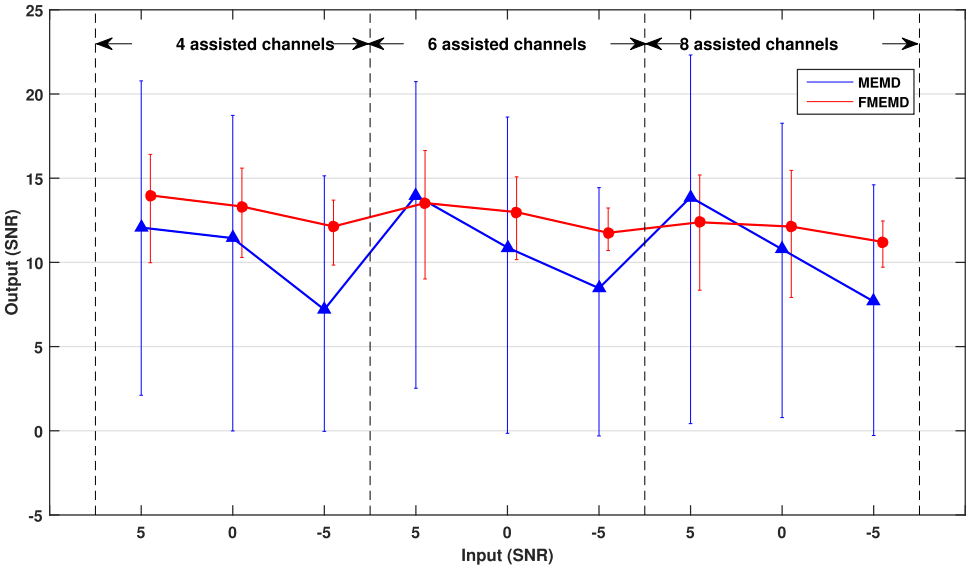

Fig. 3 The estimation results to the 6Hz sinusoidal signal by MEMD (blue lines) and FMEMD (red lines)

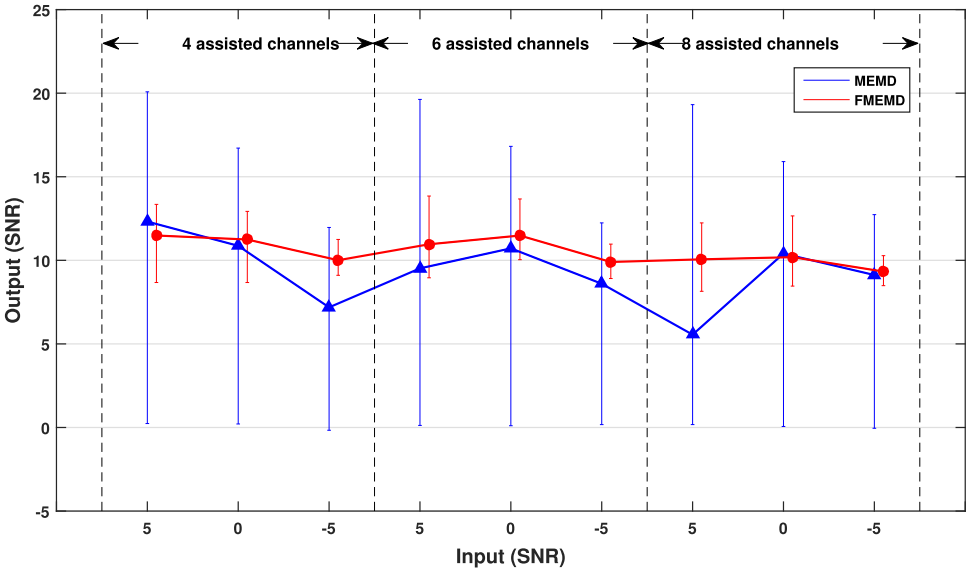

Fig. 4 The estimation results to the 15Hz sinusoidal signal by MEMD (blue lines) and FMEMD (red lines)

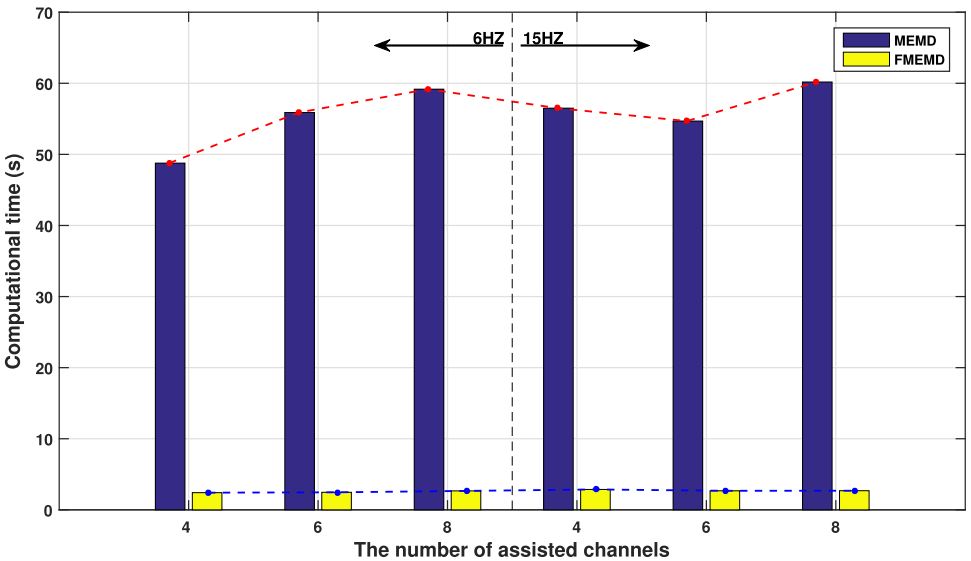

Fig. 5 The average computational times of MEMD and FMEMD corresponding to different total numbers of data channels when the 6 Hz or 15 Hz sinusoidal signals are extracted

4.2 Time–frequency analysis using FMEMD and MEMD

As mentioned before, we only choose MEMD for comparison as the researchers have illustrated its superiority on time–frequency analysis over other existing univariate methods. Both MEMD and FMEMD decompose 11 data channels with the aid of two additional noise channels, while only the analysis results of the ipsilateral hemisphere (C3 data channel) and the contralateral hemisphere (C4 data channel) with respect to the left hand motor imagery task are displayed.

The extracted *mu* and *beta* separated rhythm time series from −2 to 6 s using NA-MEMD and NA-FMEMD are shown in Fig. 6. Note that the first 2 s and last 2 s correspond to the fixed-cross and the blank screen, respectively, while the middle 4s is the duration of motor imagery task. In order to highlight the ERD and ERS, all time series display the amplitude changes relative to the mean amplitude of the first 2 s baseline interval, which are normalized in advance by the standard deviation of the baseline signal. As mentioned in [56, 57], once the subject starts to perform motor imagery task, the amplitudes decrease (ERD) for approximately 2 s over the contralateral scalp and the amplitudes increase (ERS) after 2 s over the ipsilateral scalp in the specific rhythms, especially *mu* rhythm.

According to the extracted *mu* and *beta* separated rhythms by NA-MEMD and NA-FMEMD, the ERD appears between 1.5 and 4 s over the contralateral scalp (C4 electrode), while the ERS happens around 3s over the ipsilateral scalp (C3 electrode). In particular, the *mu* separated rhythm contains more prominent ERD and ERS phenomenons than the *beta* separated rhythm, which is consistent with the above prior knowledge. Besides, compared with NA-MEMD, NA-FMEMD observes clearer ERS (around 3 s) within the *mu* and *beta* separated rhythms. Similar results are also shown by the power changes of the time series in Fig. 7. The instantaneous powers are computed by the envelopes of the time series.

Figure 8 shows the time–frequency spectra obtained by NA-MEMD and NA-FMEMD, where the motor imagery start from 0 to 4 s. The results are derived by decomposing the 11-channel EEG data of left hand motor imagery and computing the Hilbert-Huang spectra (HHS) from IMFs corresponding to C3 and C4.

As with the previous analysis results, the time–frequency spectra of NA-MEMD and NA-FMEMD show the ERS around 3 s and ERD between 1.5 and 4 s. Compared with the classic univariate methods, MEMD has been proved to provide the more localized time–frequency representations of EEG data (Park et al. 38). In this case, FMEMD also exhibits the similar ability according to Fig. 8. The difference is that FMEMD preserves less high-frequency (over 30 Hz) noise in the obtained spectra than MEMD, which generates the clearer analysis results with respect to the brain activities of left hand motor imagery.

4.3 Average preprocessing times of FMEMD and MEMD

Another comparative experiment is conducted by computing the average running time of NA-MEMD and NA-FMEMD for all trials of each subject in BCI Competition IV Dataset I. The EEG data with diverse data channels of 4, 11 and 59 (as mentioned in Sect. 4.1) are processed by NA-MEMD and NA-FMEMD. The related parameters of the applied methods are consistent with the previous section. Table 1 shows the final results. Observe that the increase in the total numbers of data channels causes less impact on the running efficiency of FMEMD than MEMD. Moreover, FMEMD improves the preprocessing time by more than 15 times compared with MEMD. Hence, FMEMD becomes more compatible with the real-world BCI systems. On the other hand, the scheme to consider the cross-channel information of more data channels simultaneously is more practicable on FMEMD due to its high calculation rate. Combining the more superior noise robustness given by the stable filter bank property, the FMEMD-based method can provide more accurate estimation of brain responses within specific frequency bands over existing methods, thereby improving the classification accuracy of motor imagery tasks.

5 Classification of motor imagery task using FMEMD

In this section, we propose a FMEMD-based classification method and evaluate it using two motor imagery datasets.

5.1 Materials

As mentioned before, we have chosen the BCI Competition IV Dataset I to evaluate the time–frequency analysis ability of FMEMD. In this section, this dataset is also used to verify the classification performance of the FMEMD-based approach over other existing methods that have employed the same dataset. Another representative dataset from the Physiobank Motor/Mental Imagery (MMI) database is taken into consideration (Schalk et al. 48). The dataset consists of a total of 109 subjects who performed the left and right hand motor imagery tasks. Each subject perform 45 trials and imagined one of two tasks for a duration of 4 s. The 64-channel EEG data are recorded at 160 Hz. Note that we exclude the data of 4 subjects including *S*088, *S*092, *S*100, and *S*104, since they had damaged recordings and too little samples (Kim et al. 21). Therefore, totally 105 subjects are considered into this classification experiment. Out of 64 EEG channels, 11 are

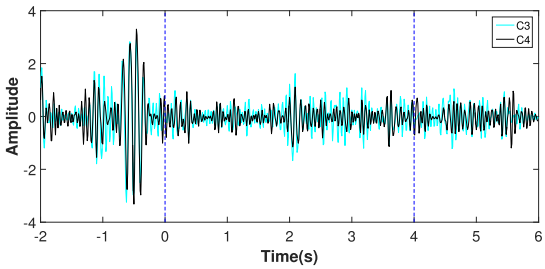

(a) *beta* rhythms using the NA-MEMD.

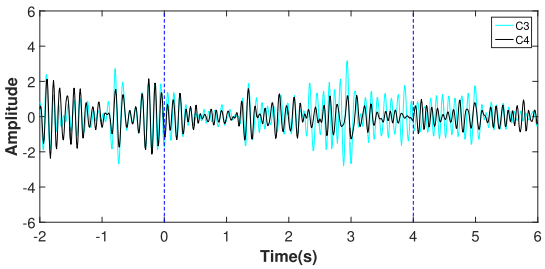

(b) *mu* rhythms using the NA-MEMD.

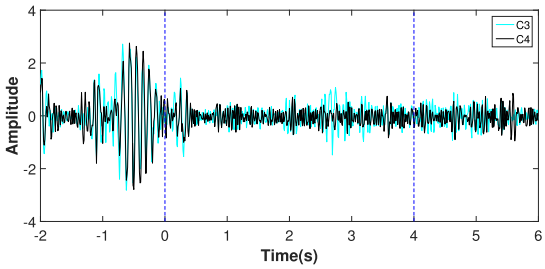

(c) *beta* rhythms using the NA-FMEMD.

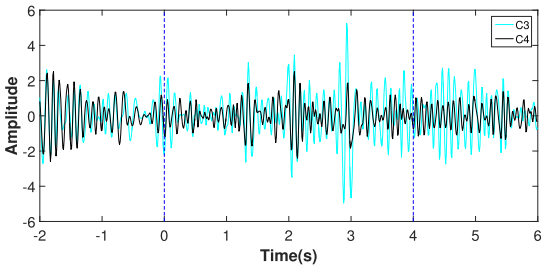

(d) *mu* rhythms using the NA-FMEMD.

Fig. 6 Amplitude changes in *beta* and *mu* rhythms normalized by the mean and standard deviation of baseline waveform, are estimated by NA-MEMD and NA-FMEMD. From 1.5 to 4 s, ERS (amplitude increase) in C3 and ERD (amplitude decrease) in C4 can be accurately observed by NA-FMEMD

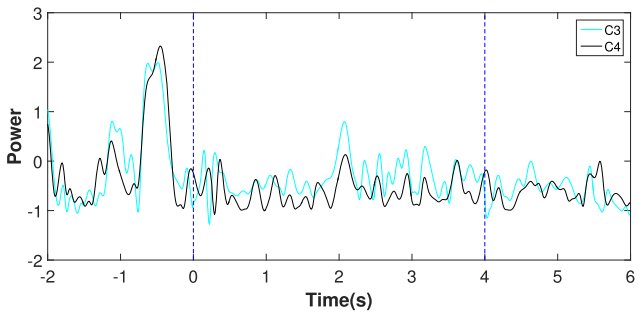

(a) Changes in *beta* power using the NA-MEMD.

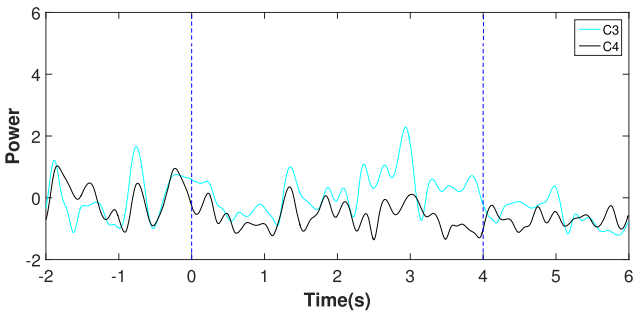

(b) Changes in *alpha* power using the NA-MEMD.

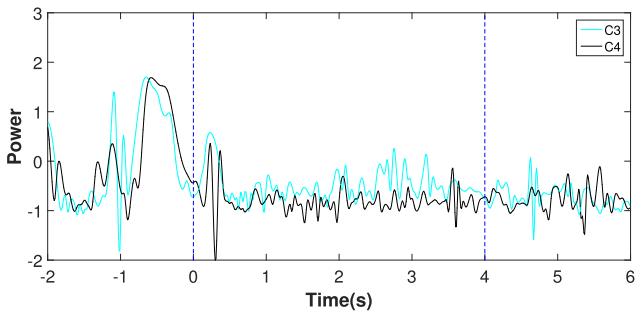

(c) Changes in *beta* power using the NA-FMEMD.

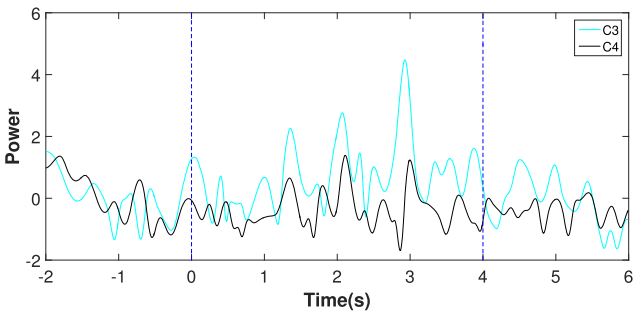

(d) Changes in *alpha* power using the NA-FMEMD.

Fig. 7 Power changes in *beta* and *mu* rhythms are estimated by NA-MEMD and NA-FMEMD. From 1.5 to 4 s, ERS (amplitude increase) in C3 and ERD (amplitude decrease) in C4 can be accurately noted by NA-FMEMD

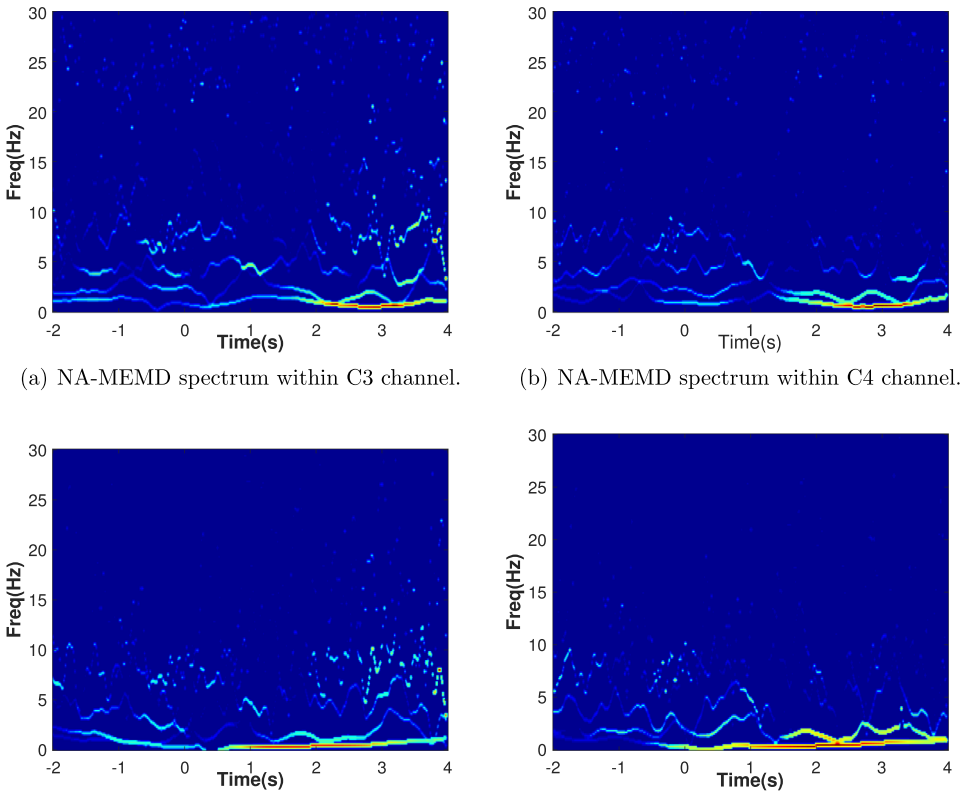

Fig. 8 NA-MEMD and NA-FMEMD spectra within the ipsilateral and contralateral scalps (C3 and C4) for left hand motor imagery tasks

(a) NA-MEMD spectrum within C3 channel.

(b) NA-MEMD spectrum within C4 channel.

(c) NA-FMEMD spectrum within C3 channel.

(d) NA-FMEMD spectrum within C4 channel.

chosen for analysis, including "FC3", "FC4", "Cz", "C3", "C4", "C5", "C6", "T7", "T8", "CP3", and "CP4". The BCI Competition IV Dataset 2a is also considered to comprehensively evaluate the performance of the proposed method. This dataset includes the EEG signals of four-category MI recognition tasks (left hand, right hand, feet, tongue) from 9 subjects. For each subject, two sessions of EEG signals were collected on different days, and there were total 288 trials (72 trials per class) per session. In accordance with the prompt displayed on the screen, four distinct MI tasks were performed by the subjects. The sampling frequency of the EEG signals from 22 electrodes was 250 Hz.

5.2 FMEMD-based classification method

5.2.1 Preprocessing

The motor imagery data from the given datasets are filtered into the different frequency modes using NA-FMEMD. As before, NA-FMEMD is applied to decompose the multi-channel EEG data simultaneously with two additional noise channels. Note that, in order to examine the relationship between the number of EEG channels and the FMEMD performance, we select the EEG data with 4, 11 and 59 channels to conduct the classification experiments. The parameters of FMEMD itself remain the same as the previous content.

Once a set of MIMFs are obtained, we need to identify the specific components and their frequency ranges which contribute to the *beta* and *mu* rhythms. One of contributions of our work is to develop an automatic screening method of frequency modes by computing the joint mean frequency of each MIMF.

For a multivariate modulated oscillation (MIMF), the joint instantaneous frequency $\omega(t)$ is defined as

$$\omega(t) = \frac{\sum_{n=0}^{N} a_n^2(t)\omega_n(t)}{\sum_{n=1}^{N} a_n^2(t)}, \tag{5}$$

which is the power-weighted average of the frequencies $\omega_n(t)$ of all N channels. Therein, $a_n(t)$ denotes the instantaneous amplitudes of each channel, while the instantaneous powers are represented as $a_n^2(t)$. This joint instantaneous frequency $\omega(t)$ is the generalization of the concept of univariate instantaneous frequency, which has been interpreted specifically in [28, 29] and [6]. The joint mean frequency $\bar{\omega}$ for each MIMF is then computed by,

$$\bar{\omega} = \frac{1}{L}\sum_{t=1}^{L}\omega(t), \tag{6}$$

Table 1 Average computational time (s) against diverse data channels

Subject	Channel	MEMD	FMEMD
a	4	3.24	0.26
	11	4.74	0.27
	59	10.06	1.12
b	4	3.23	0.25
	11	4.70	0.26
	59	10.24	1.09
f	4	3.17	0.26
	11	4.71	0.26
	59	10.43	1.09
g	4	3.17	0.30
	11	4.61	0.26
	59	10.46	1.10
Average	4	3.203	0.267
	11	4.690	0.263
	59	10.298	1.100

where L is the data length. In fact, these mean frequencies of MIMFs can be also regarded as the center frequencies of the power spectrum in the frequency domain. Using these center frequencies, we can automatically select the frequency modes corresponding to *beta* (18–25 Hz) and *mu* (8–12 Hz) rhythms, thereby enhancing the characteristics of the motor imagery responses.

5.2.2 Common spatial patterns

The common spatial patterns (CSP) approach is widely used as an effective tool to extract numerical features relevant to motor imagery responses in BCI applications (Kevric and Subasi 20, Schalk et al. 49). It aims at finding linear spatial filters that maximize the variance of EEG signals from one class while minimizing their variance from others (Lotte and Guan 31). In particular, ERD(S) caused by changing mental/brain states can be detected by CSP filters as the relative operations are sensitive to power changes of time series. A ith trial EEG data for one task C is denoted as an $N \times K$ matrix $\mathrm{X}_{i,C}$, where N is the number of channels and K represents the total number of selected MIMFs. Then details of the CSP method are presented in Algorithm 4.

Algorithm 4 Common Spatial Patterns.

1: For the total number φ_C of trials, compute the averaged normalized spatial covariance of one task as

$$\bar{R}_C = \frac{1}{\varphi_C} \sum\nolimits_{i \in \varphi_C} \frac{\bar{\mathrm{X}}_{i,C} \bar{\mathrm{X}}_{i,C}^T}{trace(\bar{\mathrm{X}}_{i,C} \bar{\mathrm{X}}_{i,C}^T)}. \tag{8}$$

Note that only two tasks are classified in this work, i.e., left hand and right hand motor imagery of subject g. Thus, their corresponding covariance matrix are denoted as $\bar{R}_l$ and $\bar{R}_r$, respectively;

2: The composite spatial covariance is given by

$$R = \bar{R}_l + \bar{R}_r. \tag{9}$$

Then R is factored as $R = U_0 \lambda {U_o}^T$, where U_0 is the matrix of eigenvectors, and λ represents the diagonal matrix of eigenvalues;

3: Perform whitening operations $S_l = P \bar{R}_l P^T$ and $S_r = P \bar{R}_r P^T$ using the eigenvalue matrix $P = \sqrt{\lambda} {U_o}^T$;

4: Obtain the common eigenvector matrix U_s and the respective eigenvalue λ_l as well as λ_r through the factorizations of S_l and S_r matrix, as shown below

$$S_l = U_s \lambda_l {U_s}^T, S_r = U_s \lambda_r {U_s}^T, \lambda_l + \lambda_r = I. \tag{10}$$

5: Based on the results from 3 and 4, the final spatial filter is derived via $W = {U_s}^T P$. This allows us to project the EEG signals as,

$$Z_{i,C} = W X_{i,C}, \tag{11}$$

where the subscript i signifies ith trial of one task and C denotes left or right hand motor imagery task.

6: Select the m first and last rows of $Z_{i,C}$ to compute the features of interest υ_p^C using

$$\upsilon_{i,p}^C = \log \left(\frac{\mathrm{var}(Z_{i,p})}{\sum_{j=1,\ldots m, N-m+1,\ldots,N} \mathrm{var}(Z_{i,j})} \right), \tag{12}$$

thus generating the feature vector as $F_i^C = [\upsilon_{i,1}^C, \upsilon_{i,2}^C, \ldots, \upsilon_{i,p}^C, \ldots, \upsilon_{i,2m}^C]$ with regard to a single trial of one task.

5.2.3 Classification

In this work, the feature vectors, which are yielded by Eq. 6 in Algorithm 4 for $m = 1, 2$, are classified using different classifiers. Both the linear discriminant analysis (LDA) and support vector machine (SVM) algorithms[2] were, and still are, the most popular types of classifiers for EEG based-BCIs, particularly for online and real-time BCIs (Lotte et al. 32). Therefore, we select these two representative classifiers to perform the classification tasks, while exploring the impact of different classifiers on the FMEMD-based classification

[2] The implementations of LDA and SVM in the MATLAB Classification Learner App are used in this paper.

performance. We divide 200 trial data for each subject from BCI Competition IV Dataset I into 140 training and 60 testing sets, and the 45 trial data in Physiobank MMI database into 32 subjects for training and 13 for test sets.[3]

The classification performance of all classifiers are calculated using a five-cross validation, while the classification tasks of each subject are repeated for 100 times by mixing the sample order. It is worth noting that the upper limit of confidence intervals between two classes corresponding to the number of trials was 56.9% for 200 trails and 64.0% for 45 trails (Kim et al. 21, Loboda et al. 30). Only the subjects with classification rates over 56.9% or 64.0% are categorized as significant subjects to display.

The architecture of FMEMD-based classification method is given by Fig. 9.

Note that, instead of reconstructing the EEG data by calculating the sum of the selected MIMFs (Gaur et al. 13, Park et al. 38), we conduct the feature extractions with respect to different frequency sub-bands using common spatial pattern filters (CSP), respectively, and integrate these features into a feature vector. This further highlights the advantages of FMEMD in terms of frequency band separation and mode alignment, while enabling the feature vectors to contain more information on brain activities.

5.3 Results

Table 2 shows the classification performances for the four subjects of BCI Competition IV Dataset I using NA-FMEMD, NA-MEMD along with LDA and SVM classifiers.

The proposed method-1 applies NA-FMEMD to 11-channel EEG data for all subjects(NA-FMEMD+CSP+LDA (11)), and extract the feature vectors using CSP, then achieving the classification with LDA classifier. In order to examine the impact of data channels on the classification performance of FMEMD-based methods, 59-channel EEG data are used in the proposed method-2(NA-FMEMD+CSP+LDA(59)). Besides this, the Method-3 classifies the CSP features from the 11-channel EEG data using SVM(NA-FMEMD+CSP+SVM(11)), thereby realizing the comparison between different classifiers. The above three methods all make use of the proposed FMEMD-based architecture.

As we can see that since Method-2 considers the information from more data channels, it achieves the improvement of 2.5%, 1.2%, and 1.2% for three subjects (a, b, and f) over Method-1. However, the accuracy of Method-2 for subject g is much lower than Method-1. This may be because the features of subject g are more concentrated on the selected 11 channels, while the remaining channels cause

[3] The parameters of CSP filters are generated by only the training data sets.

Table 2 Classification results (%) for four subjects of BCI competition IV dataset I using all applied algorithms

Subject	NA-FMEMD+CSP+LDA(11)	NA-FMEMD+CSP+LDA(59)	NA-FMEMD+CSP+SVM(11)	MEMD+CSP+SVM	FBCSP+SVM	CSP-TSM+SVM	DRL1-CSP
a	83.6 ± 6.8	86.1 ± 6.0	83.3 ± 5.9	85.9 ± 3.9	80.9 ± 9.4	88.1 ± 6.6	64.5
b	76.6 ± 4.1	77.8 ± 4.8	76.3 ± 3.7	78.7 ± 3.7	55.3 ± 11.3	59.1 ± 10.3	62.0
f	82.1 ± 5.9	83.3 ± 6.1	82.0 ± 5.0	78.8 ± 4.4	80.4 ± 8.5	85.9 ± 7.1	60.5
g	92.0 ± 4.5	83.1 ± 5.9	90.9 ± 3.9	91.9 ± 3.0	93.1 ± 6.6	92.2 ± 5.7	85.0
Average	83.6 ± 4.5	82.6 ± 5.9	83.1 ± 4.6	83.8 ± 3.8	77.4 ± 8.9	81.3 ± 7.4	68.0 ± 11.5

Proposed method 1, 2 and 3 all employ the FMEMD-based architecture. Method-1 shows the results using 11-channel EEG data with LDA classifier (NA-FMEMD+CSP+LDA(11)), while Method-2 processes 59-channel data (NA-FMEMD+CSP+LDA(59)). The comparison between different classifiers is conducted on Method-1 and Method-3, since Method-3 uses SVM with the same 11-channel data (NA-FMEMD+CSP+SVM(11)). Three recently proposed methods that utilize the same dataset, namely Method-4 (MEMD-based CSP with SVM) (Park et al. 38), Method-5 (FBCSP with SVM) (Kumar et al. 22), Method-6 (CSP-TSM with SVM) (Kumar et al. 23), and Method-7 (DRL1-CSP) (Jin et al. 19), are also taken into consideration. The best results are given for all subjects

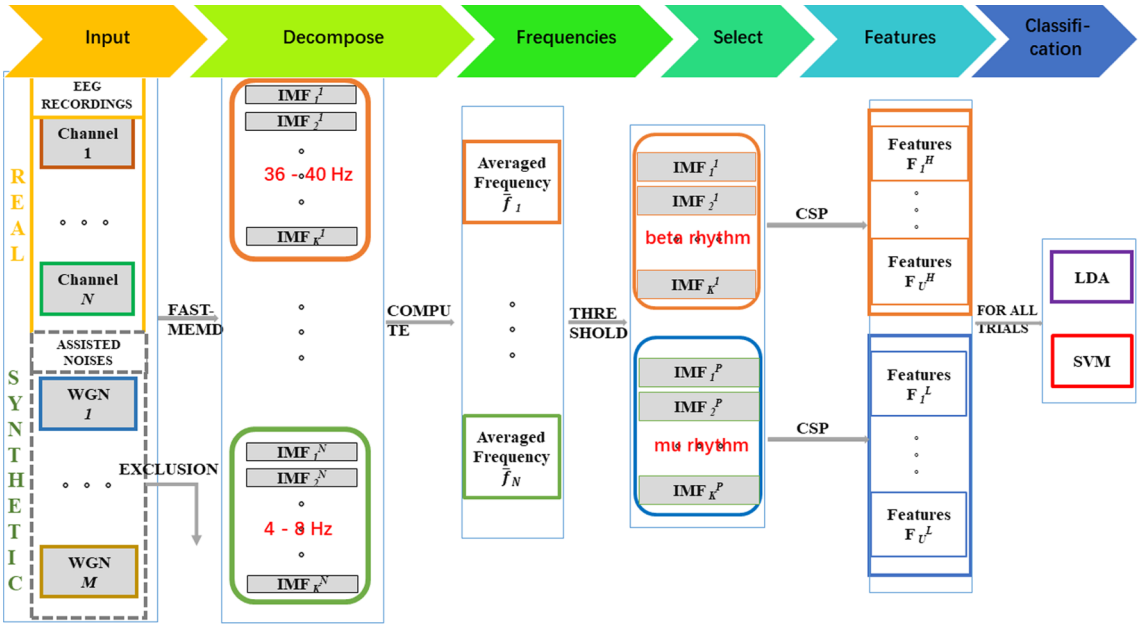

Fig. 9 Architecture of the proposed FMEMD-based classification approach for left and right hand motor imagery tasks

the adverse effect on the feature extraction. Compared with Method-3, Method-1 shows a more superior performance for all subjects, which reveals that the LDA classifier is more suitable for FMEMD-based method. On average, the best and robustest performance is obtained by Method-1, where it achieves a 1.0% improvement over Method-2, a 0.5% improvement over Method-3.

Table 2 also shows the comparison with other state-of-art methods, including Method-4 (MEMD-based CSP with SVM) (Park et al. 38), Method-5 (FBCSP with SVM) (Kumar et al. 22), Method-6 (CSP-TSM with SVM) (Kumar et al. 23) and Method-7(DRL1-CSP) (Jin et al. 19). The Method-4 exploited NA-MEMD to filter the 11-channel EEG data. Then it computed the CSP features from manually selected decomposition components, further classified by SVM. Method-5 and Method-6 applied a butterworth bandpass filter to raw EEG data, and performed the feature extraction stage using FBCSP and CSP-TSM (CSP and tangent space mapping (TSM)), respectively. These features are then classified by the same SVM classifier. Method-7 applied a internal feature selection for CSP based on Difference and Ratio of Average L1-Norm.Observe that our proposed method can maintain superior classification performances for all subjects over other methods. On average, the NA-FMEMD-based method gives the high accuracies of 83.6%, a 6.2% improvement over Method-5 (FBCSP with SVM), a 2.3% improvement over Method-6 (CSP-TSM with SVM), and a 15.6% improvement over Method-7(DRL1-CSP). Although Method-4 (NA-MEMD-based method) marginally outperforms Method-1 by 0.2%, the running rate of the proposed method is 20 times more than Method-4 (see also Sect. 4.3 and Table 1), which benefits real-time BCIs.

The classification rates for the second dataset, Physiobank MMI database, are obtained by NA-FMEMD and NA-MEMD with CSP, which are shown in Table 4. Among FMEMD-based approaches, we chose Proposed Method-1 since it showed the better-synthesized performance in the experiment of BCI Competition IV Dataset I over proposed Method-2 and Method-3. The NA-MEMD-based method is still denoted as Method-4. Followed by [38], we also displayed ten subjects for a detailed comparison. Except for two subjects 25 and 12, Method-1 showed the best classification accuracies for the remaining eight subjects. On average, the proposed method gave a 0.9% improvement over NA-MEMD (Method-4).

Table 3 shows the average classification rates for all significant subjects obtained by the proposed method and other existing approaches. Observe that our proposed method presents a comparable performance over other methods. Although the FMEMD-based method in this work achieves a slightly lower accuracy compared to the works in [21] and [11], we should notice that: (1) the former still uses MEMD to preprocessing EEG data, which consumes plenty of running time, especially when the number of data channels increases. Researchers have illustrated that the SUT-CCSP (strong-uncorrelating transform based complex CSP) used in this method shows more superior performance in terms of feature extraction than the conventional CSP used in our proposed method (Park et al. 39). Therefore, the new method combining NA-FMEMD with SUT-CCSP may achieve better performance than MEMD-based one; (2) the latter method

Table 3 Overview over other works performing motor imagery classification tasks on the Physiobank MMI dataset for all subjects, and comparison to this work's results

Work	Number of channels	Accuracy	Methods
[39]	58	72.37%	SUT-CCSP + SVM
[21]	14	80.05%	MEMD + SUT-CCSP + Random forest
[52]	3	68.21%	Wavelet transform + DNN
[11]	14	82.66%	CNN
This work	11	78.60%	NA-FMEMD + CSP + LDA

Table 4 Classification Results (%) for ten subjects of Physiobank MMI database using Proposed Method-1 and Method-4

Subject	NA-FMEMD+CSP+LDA(11)	MEMD-CSP-SVM
1	79.0 ± 10.9	77.2 ± 9.7
2	88.5 ± 7.0	86.0 ± 9.1
4	69.2 ± 11.2	66.4 ± 10.6
7	97.9 ± 5.2	97.1 ± 4.9
12	62.6 ± 10.7	64.0 ± 13.1
13	71.2 ± 13.7	65.5 ± 11.3
15	72.4 ± 11.6	71.2 ± 12.1
25	71.0 ± 10.7	77.6 ± 10.9
26	75.1 ± 12.5	74.2 ± 12.0
29	98.9 ± 3.7	97.4 ± 4.0
Average	78.6 ± 9.7	77.7 ± 9.8

Method-1 shows the results using 11-channel EEG data with LDA classifier, while Method-4 utilizes NA-MEMD and CSP for feature extraction, and classifies these features by SVM (Park et al. 38). The best results are given for all subjects

Table 5 Overview over other works performing motor imagery classification tasks on the BCI Competition IV Dataset 2a for all subjects, and comparison to this work's results

Work	Accuracy	Methods
	61.96%	Shallow CNN
[50]	62.15%	Deep CNN
[25]	63.50%	EEGNet
[34]	62.00%	FBCNet
[1]	62.57%	ATCNet
This work	62.43%	NA-FMEMD + CSP + LDA

based on convolution neural network (CNN) is an end-to-end learning approach for classification of motor imagery tasks. It requires a lot of high-quality training data while showing poor model interpretability, which leads to the low compatibility with practical BCI systems. Besides, this method also lacks verification of other data sets.

Table 5 shows the average classification rates on the BCI Competition IV Dataset 2a obtained by the proposed method and popular deep learning methods. Observe that our proposed method presents a comparable performance over other methods. Although the FMEMD-based method in this work achieves a slightly lower accuracy compared to the EEGNet and ATCNet, it still surpasses most other deep learning methods. These end-to-end learning approaches for classification of motor imagery tasks requires a lot of high-quality training data while showing poor model interpretability, which leads to the low compatibility with practical BCI systems.

Therefore, among the reviewed methods for the classification of motor imagery tasks, our proposed one is a real-time BCI oriented approach with the best-synthetic performance. While it is true that utilizing deep learning methods can enhance accuracy, FMEMD as a preprocessing method can also be incorporated into neural network models to replace segmentation filtering like FBCSP. We will conduct relevant research in our future work.

5.4 Discussion

In this paper, we applied our recently proposed FMEMD method to analyze motor imagery EEG data. FMEMD inherited the ability of MEMD to multivariate analysis, thereby providing a scale-alignment decomposition and physically meaningful component estimations for motor imagery response. It is cleared that FMEMD showed higher noise robustness due to its fairly stable filter bank property compared with MEMD. Hence, there is no obvious mode mixing and mode misalignment problems are introduced by FMEMD. Besides, it achieved more precise and stable multivariate component estimations under the disturbances of White Gaussian noises with different SNR. The above statements were verify in Sect. 3 (simulation data) and Sect. 4 (real-world data). More specifically, Figs. 1, 2, 3, and 4 clearly revealed a more superior decomposition performance exhibited by FMEMD in terms of mode mixing and component estimation. Particularly, the fewer fluctuations of estimation results using FMEMD (as shown in Figs. 3 and 4) among all repeated trials for each frequency mode in the component estimation experiment again illustrated its stable filter bank property. For the real-world two-channel EEG data from BCI Competition IV Dataset I, FMEMD also observed more prominent ERD and ERS phenomenons from both views of instantaneous amplitudes (Fig. 6) and instantaneous powers (Fig. 7). Therefore, the power spectra yielded by FMEMD not only showed similar enhanced-localization characteristics, but also exhibited the less high-frequency noisy points than MEMD in the time–frequency plane (see also Fig. 8).

It was shown that FMEMD enhanced noise robustness in the improvement of classification rates on two typical datasets, especially Physiobank MMI dataset (see Table 4). For the displayed ten subjects, the FMEMD-based method basically maintained the better classification results than MEMD, which demonstrated that FMEMD retained more accurate cross-channel information for each subject. For the first dataset BCI Competition IV Dataset I, the FMEMD-based method outperformed most applied methods, except for showing a slightly lower average classification rate then MEMD (see Table 2). However, the higher computational efficiency of FMEMD compensates for this drawback in the sense of real-time BCIs.

Figure 5 (simulation data which is similar to rhythms) and Table 1 (EEG data with different channels) revealed that the existing time of FMEMD for processing multichannel data was much shorter than MEMD, and, in particular, this superiority became more obvious when the total number of data channels increased. The greatly reduced computational load of FMEMD led to the enhanced compatibility with practical and real-time BCI systems. In addition, FMEMD allowed the simultaneous analysis of more channels without the apprehension of increased running time from more data channels. It showed that more EEG information corresponding to other channels was taken into consideration, which may resulted in the improved classification performance. In fact, the comparison of the classification accuracies of proposed Method-1 (with 11-channel EEG) and Method-2 (with 59-channel EEG) on subjects a, b, and f in Table 2 verified this statement.

In this work, we also introduced a more physically meaningful screening index of frequency modes than frequency measures used in [13]. The index for each MIMF is computed by averaging the joint instantaneous frequencies across data channels. The related information about the joint instantaneous frequencies of a multivariate modulated oscillation can be found in [28, 29]. Combining the newly proposed selecting strategy, we developed the FMEMD-based classification scheme, as shown in Fig. 9. However, although our proposed scheme was comparable to other hybrid methods, it failed to show the highest classification rates (see Table 3) since the feature extraction method and classifier used in this work were not further analyzed and optimized. We can find several effective directions for improving the overall performance from the experimental results. For examples, LDA classifier was more suitable for the FMEMD-based method than SVM, as verified by the classification results of proposed Method-2 and Method-3 in Table 2. Researchers have illustrated that the nonlinear classifier, such as random forest (RF) can produce more superior performance than conventional classifiers (like LDA) in the application of motor imagery classification (Kim et al. 21). This finding may also significantly improve the FMEMD-based classification method. On the other hand, a suitable selection strategy of data channel is essential for our proposed method. Overly more data channels sometimes will damage the extracted EEG features, thereby resulting in less accuracies for certain subjects. The lower classification rate of proposed Method-2 on subject g illustrated this point (see also Table 2). Fortunately, the EEG channel selection scheme is already a relatively mature technology, moreover, FMEMD does not need to consider the impact of the number of channels on the operating efficiency, thus being expected to further obtain more superior performance of the FMEMD-based method. It is indicated that FMEMD architecture is not limited to motor imagery cases but can also be employed in the analysis of several neural data. A new area of research has arisen pertaining to the separation and parametrization of neural oscillations (Donoghue et al. 10), and this method can make contribution to the development of this field.

6 Conclusion

In this study, our recently proposed FMEMD method has been explored to EEG rhythm separation and time–frequency analysis compared with other state-of-art methods. It was found that FMEMD and its noise-assisted version can significantly improve classification performance on BCI Competition IV dataset and attained a comparable performance to complex methods on the Physiobank MMI dataset and BCI Competition IV 2a dataset within less executing time. The stable filter bank property and low computational complexity of FMEMD enable its accurate component estimation and high noise robustness, thus providing more accurate brain activities corresponding to the specific frequency bands, especially *mu* and *beta* rhythms. Future works will concentrate on the improvement of the FMEMD-based method and its implementation. Our intention is to utilize FMEMD architecture as a novel approach for EEG rhythm separation to investigate the mechanisms of neurological disorders, aid in their diagnosis, and conduct classification research on various cognitive tasks.

Acknowledgements The authors wish to thank sponsor and financial support from National Natural Science Foundation of P.R. China (Grant Nos. 61134007, 61374121), the 111 Project (Grant No. B07031), and the Shenzhen Science and Technology Program (Grant No. KQTD20200820113106007).

Author contributions Yang Jiao and Qian Zheng wrote the main manuscript text and prepared most of figures. Yi pan provides our project funding. Lei Xie, Xun Lang and Dan Qiao assist in finishing table1 and table2. All authors reviewed the manuscript.

Declarations

Conflicts of interest The authors declare no competing interests.

References

1. Altaheri H, Muhammad G, Alsulaiman M (2022) Physics-informed attention temporal convolutional network for EEG-based motor imagery classification. IEEE Trans Ind Inf 19(2):2249–58
2. Anderson CW, Stolz EA, Shamsunder S (1998) Multivariate autoregressive models for classification of spontaneous electroencephalographic signals during mental tasks. IEEE Trans Biomed Eng 45(3):277–86
3. Ang KK, Chin ZY, Zhang H, Guan C (2008) Filter bank common spatial pattern (FBCSP) in brain-computer interface. In: 2008 IEEE international joint conference on neural networks (IEEE world congress on computational intelligence). IEEE, pp 2390–2397
4. Bashar SK, Bhuiyan MIH (2016) Classification of motor imagery movements using multivariate empirical mode decomposition and short time Fourier transform based hybrid method. Eng Sci Technol Int J 19(3):1457–64
5. Blankertz B, Dornhege G, Krauledat M, Müller KR, Curio G (2007) The non-invasive Berlin brain-computer interface: fast acquisition of effective performance in untrained subjects. Neuroimage 37(2):539–50
6. Boashash B (1992) Estimating and interpreting the instantaneous frequency of a signal. I. Fundamentals. Proc IEEE 80(4):520–38
7. Bostanov V, Kotchoubey B (2004) Recognition of affective prosody: continuous wavelet measures of event-related brain potentials to emotional exclamations. Psychophysiology 41(2):259–68
8. Craik A, He Y, Contreras-Vidal JL (2019) Deep learning for electroencephalogram (EEG) classification tasks: a review. J Neural Eng 16(3):031001
9. Dai M, Zheng D, Na R, Wang S, Zhang S (2019) EEG classification of motor imagery using a novel deep learning framework. Sensors 19(3):551
10. Donoghue T, Haller M, Peterson EJ, Varma P, Sebastian P, Gao R et al (2020) Parameterizing neural power spectra into periodic and aperiodic components. Nat Neurosci 23(12):1655–65
11. Dose H, Møller JS, Iversen HK, Puthusserypady S (2018) An end-to-end deep learning approach to MI-EEG signal classification for BCIs. Expert Syst Appl 114:532–42
12. Doud AJ, Lucas JP, Pisansky MT, He B (2011) Continuous three-dimensional control of a virtual helicopter using a motor imagery based brain–computer interface. PLoS ONE 6(10):e26322
13. Gaur P, Pachori RB, Wang H, Prasad G (2018) A multi-class EEG-based BCI classification using multivariate empirical mode decomposition based filtering and Riemannian geometry. Expert Syst Appl 95:201–11
14. Graimann B, Allison B, Pfurtscheller G (2009) Brain–computer interfaces: a gentle introduction. In: Brain–computer interfaces. Springer, pp 1–27
15. Hernández LG, Antelis JM (2018) A comparison of deep neural network algorithms for recognition of EEG motor imagery signals. In: Mexican conference on pattern recognition. Springer, pp 126–134
16. Hu J, Xiao D, Mu Z (2009) Application of energy entropy in motor imagery EEG classification. Int J Digit Content Technol Appl 3(2):83–90
17. Huang NE, Zheng S, Long SR, Wu MC, Shih HH, Zheng Q et al (1971) The empirical mode decomposition and the Hilbert spectrum for nonlinear and non-stationary time series analysis. Proc Math Phys Eng Sci 1998(454):903–95
18. Huang NE, Wu MLC, Long SR, Shen SS, Qu W, Gloersen P et al (2003) A confidence limit for the empirical mode decomposition and Hilbert spectral analysis. Proc R Soc Lond Ser A Math Phys Eng Sci 459(2037):2317–45
19. Jin J, Xiao R, Daly L, Miao Y, Wang X, Cichock A (2020) Internal feature selection method of CSP based on L1-norm and Dempster–Shafer theory. IEEE Trans Neural Netw Learn Syst 32:4814–25
20. Kevric J, Subasi A (2017) Comparison of signal decomposition methods in classification of EEG signals for motor-imagery BCI system. Biomed Signal Process Control 31:398–406
21. Kim Y, Ryu J, Kim KK, Took CC, Mandic DP, Park C (2016) Motor imagery classification using mu and beta rhythms of EEG with strong uncorrelating transform based complex common spatial patterns. Comput Intell Neurosci 2016
22. Kumar S, Sharma A, Tsunoda T (2017) An improved discriminative filter bank selection approach for motor imagery EEG signal classification using mutual information. BMC Bioinform 18(16):545
23. Kumar S, Mamun K, Sharma A (2017) CSP-TSM: optimizing the performance of Riemannian tangent space mapping using common spatial pattern for MI-BCI. Comput Biol Med 91:231–42
24. Lang X, Zheng Q, Zhang Z, Lu S, Xie L, Horch A et al (2018) Fast multivariate empirical mode decomposition. IEEE Access 6:65521–38
25. Lawhern VJ, Solon AJ, Waytowich NR, Gordon SM, Hung CP, Lance BJ (2018) EEGNet: a compact convolutional neural network for EEG-based brain-computer interfaces. J Neural Eng 15(5):056013
26. Lebedev MA, Nicolelis MA (2006) Brain-machine interfaces: past, present and future. Trends Neurosci 29(9):536–46
27. Lemm S, Blankertz B, Curio G, Muller KR (2005) Spatio-spectral filters for improving the classification of single trial EEG. IEEE Trans Biomed Eng 52(9):1541–8
28. Lilly JM, Olhede SC (2009) Bivariate instantaneous frequency and bandwidth. IEEE Trans Signal Process 58(2):591–603
29. Lilly JM, Olhede SC (2011) Analysis of modulated multivariate oscillations. IEEE Trans Signal Process 60(2):600–12
30. Loboda A, Margineanu A, Rotariu G, Lazar AM (2014) Discrimination of EEG-based motor imagery tasks by means of a simple phase information method. Int J Adv Res Artif Intell 3(10)
31. Lotte F, Guan C (2010) Regularizing common spatial patterns to improve BCI designs: unified theory and new algorithms. IEEE Trans Biomed Eng 58(2):355–62
32. Lotte F, Bougrain L, Cichocki A, Clerc M, Congedo M, Rakotomamonjy A et al (2018) A review of classification algorithms for EEG-based brain-computer interfaces: a 10-year update. J Neural Eng 15(3):031005.1-031005.28
33. Mandic DP, ur Rehman N, Wu Z, Huang NE (2013) Empirical mode decomposition-based time-frequency analysis of multivariate signals: the power of adaptive data analysis. IEEE Signal Process Mag 30(6):74–86
34. Mane R, Chew E, Chua K, Ang KK, Robinson N, Vinod AP et al (2021) FBCNet: a multi-view convolutional neural network for brain-computer interface. arXiv preprint arXiv:2104.01233
35. Mousavi EA, Maller JJ, Fitzgerald PB, Lithgow BJ (2011) Wavelet common spatial pattern in asynchronous offline brain computer interfaces. Biomed Signal Process Control 6(2):121–8
36. Nicolas-Alonso LF, Gomez-Gil J (2012) Brain computer interfaces, a review. Sensors 12(2):1211–79
37. Park C, Looney D, Kidmose P, Ungstrup M, Mandic DP (2011) Time-frequency analysis of EEG asymmetry using bivariate empirical mode decomposition. IEEE Trans Neural Syst Rehabil Eng 19(4):366–73
38. Park C, Looney D, Rehman NU, Ahrabian A, Mandic DP (2013) Classification of motor imagery BCI using multivariate empirical mode decomposition. IEEE Trans Neural Syst Rehabil Eng 21(1):10–22
39. Park C, Took CC, Mandic DP (2013) Augmented complex common spatial patterns for classification of noncircular EEG from motor imagery tasks. IEEE Trans Neural Syst Rehabil Eng 22(1):1–10

40. Park C, Plank M, Snider J, Kim S, Huang HC, Gepshtein S et al (2014) EEG gamma band oscillations differentiate the planning of spatially directed movements of the arm versus eye: multivariate empirical mode decomposition analysis. IEEE Trans Neural Syst Rehabil Eng 22(5):1083–96
41. Pfurtscheller G, Neuper C, Flotzinger D, Pregenzer M (1997) EEG-based discrimination between imagination of right and left hand movement. Electroencephalogr Clin Neurophysiol 103(6):642–51
42. Pfurtscheller G, Brunner C, Schlögl A, Da Silva FL (2006) Mu rhythm (de) synchronization and EEG single-trial classification of different motor imagery tasks. Neuroimage 31(1):153–9
43. Ramoser H, Muller-Gerking J, Pfurtscheller G (2000) Optimal spatial filtering of single trial EEG during imagined hand movement. IEEE Trans Rehabil Eng 8(4):441–6
44. Rehman N, Mandic DP (2010) Multivariate empirical mode decomposition. Proc Math Phys Eng Sci 466(2117):1291–302
45. Rehman N, Naveed K, Safdar M, Ehsan S, McDonald-Maier K (2015) Dynamically sampled multivariate empirical mode decomposition. Electron Lett 51(24):2049–51
46. Rilling G, Flandrin P, Gonçalves P, Lilly JM (2007) Bivariate empirical mode decomposition. IEEE Signal Process Lett 14(12):936–9
47. Robinson N, Vinod AP, Ang KK, Tee KP, Guan CT (2013) EEG-based classification of fast and slow hand movements using wavelet-CSP algorithm. IEEE Trans Biomed Eng 60(8):2123–32
48. Schalk G, McFarland DJ, Hinterberger T, Birbaumer N, Wolpaw JR (2004) A general-purpose brain-computer interface (BCI) system. IEEE Trans Biomed Eng 51:1034–43
49. Schalk G, McFarland DJ, Hinterberger T, Birbaumer N, Wolpaw JR (2004) BCI2000: a general-purpose brain-computer interface (BCI) system. IEEE Trans Biomed Eng 51(6):1034–43
50. Schirrmeister RT, Springenberg JT, Fiederer LDJ, Glasstetter M, Eggensperger K, Tangermann M et al (2017) Deep learning with convolutional neural networks for EEG decoding and visualization. Hum Brain Mapp 38(11):5391–420
51. Tabar YR, Halici U (2016) A novel deep learning approach for classification of EEG motor imagery signals. J Neural Eng 14(1):016003
52. Tolić M, Jović F (2013) Classification of wavelet transformed EEG signals with neural network for imagined mental and motor tasks. Kinesiol Int J Fundam Appl Kinesiol 45(1):130–8
53. Ur Rehman N, Mandic DP (2011) Filter bank property of multivariate empirical mode decomposition. IEEE Trans Signal Process 59(5):2421–6
54. Wang Z, Maier A, Logothetis NK, Liang H (2008) Single-trial classification of bistable perception by integrating empirical mode decomposition, clustering, and support vector machine. EURASIP J Adv Signal Process 2008:1–8
55. Wang P, Jiang A, Liu X, Shang J, Zhang L (2018) LSTM-based EEG classification in motor imagery tasks. IEEE Trans Neural Syst Rehabil Eng 26(11):2086–95
56. Yuan H, He B (2014) Brain-computer interfaces using sensorimotor rhythms: current state and future perspectives. IEEE Trans Biomed Eng 61(5):1425–35
57. Yuan H, Doud A, Gururajan A, He B (2008) Cortical imaging of event-related (de) synchronization during online control of brain-computer interface using minimum-norm estimates in frequency domain. IEEE Trans Neural Syst Rehabil Eng 16(5):425–31
58. Zhang Z, Duan F, Sole-Casals J, Dinares-Ferran J, Cichocki A, Yang Z et al (2019) A novel deep learning approach with data augmentation to classify motor imagery signals. IEEE Access 7:15945–54